THE JOURNAL OF
PHYSICAL CHEMISTRY C

pubs.acs.org/JPCC Article

High-Pressure Raman Study of $Fe(IO_3)_3$: Soft-Mode Behavior Driven by Coordination Changes of Iodine Atoms

Akun Liang, Saqib Rahman, Placida Rodriguez-Hernandez, Alfonso Muñoz, Francisco Javier Manjón, Gwilherm Nenert, and Daniel Errandonea*

Cite This: *J. Phys. Chem. C* 2020, 124, 21329−21337 **Read Online**

ACCESS | Metrics & More | Article Recommendations | Supporting Information

ABSTRACT: We report high-pressure Raman spectroscopy studies of $Fe(IO_3)_3$ up to nearly 21 GPa that have been interpreted with the help of density functional theory calculations, which include the calculation of phonon dispersion curves and elastic constants at different pressures. Zero-pressure Raman-active mode frequencies and their pressure dependences have been determined. Modes have been assigned and correlated to atomic movements with the help of calculations. Interestingly, in the high-frequency region, there are several modes that soften under compression. These modes have been identified as internal vibrations of the IO_3 coordination polyhedron. Their unusual behavior is a consequence of the changes induced by pressure in the coordination sphere of iodine, which gradually change from a threefold coordination to an almost sixfold coordination under compression. The coordination change is favored by the decrease of the stereoactivity of the iodine lone electron pair so that likely a real sixfold coordination is attained after a first-order phase transition previously reported to occur above 21 GPa. The strong nonlinear behavior found in Raman-active modes as well as in theoretically calculated elastic constants has been discovered to be related to the occurrence of two previously unreported isostructural phase transitions at 1.5−2.0 and 5.7−6.0 GPa as shown by dynamic instabilities close to the Brillouin zone center.

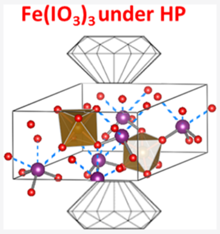

Metal iodates usually show an asymmetric coordination geometry because of the presence of lone electron pairs (LEPs) in the iodine atom. Consequently, they can form a diversity of unusual structures and many of them have multiple promising properties or applications, such as large second-harmonic generation coefficient materials,[1−4] chiral materials with second-order nonlinear optical activity in the visible and near- and mid-IR ranges,[5] and barocaloric materials.[6]

Of particular interest are compounds with the composition $M(IO_3)_3$, with M being a trivalent metal atom and iodine (I) being a pentavalent atom. These metal iodates show a diversity of unusual crystalline structures because of the asymmetric coordination geometry produced by the iodine LEP. A feature of these compounds is that IO_3 units do not form planar triangles, such as in borate (BO_3) or carbon trioxide (CO_3) units. Instead, IO_3 units are not planar and have a pyramidal form with three O atoms in the corners of the base and the iodine atom in the top corner of the pyramid. This unit can be seen in Figure 1, where the crystal structure of $Fe(IO_3)_3$ is schematically represented. In fact, the polyhedron around I could be described as an IO_3E tetrahedron, where E is the iodine LEP. Therefore, iodine can be considered as fourfold coordinated if we take into account the LEP, with iodine sitting in the center of a distorted tetrahedron where the oxygen atoms are occupying three corners and the fourth one is occupied by the lone pair of electrons of the iodine atom. It should be noted that the I−O bond distance in the IO_3E unit is of the order of 1.9 Å, while the I−O distances to the three second-next oxygen neighbors are between 2.55 and 2.95 Å (see Figure 1). We show that these atoms become relevant at high pressure (HP) to increase the coordination of I atoms and explain the changes observed in the vibrational properties of $Fe(IO_3)_3$.

It is well known that HP modifies interatomic distances, leading to changes in the physical properties of materials. This has contributed to improve the properties of materials and to several discoveries that have impacted physics, chemistry, and materials sciences. Among transition-metal iodates, such studies have been carried out only in $Fe(IO_3)_3$.[7] This material was studied by powder X-ray diffraction (XRD), IR spectroscopy, and density functional theory (DFT) simulations. It undergoes a first-order phase transition at 22 GPa, with a volume change and an abrupt change of the c/a axial ratio. The phase transition is triggered by changes in the coordination of iodine atoms, which is driven by the decrease of the stereoactivity of the iodine LEP. DFT calculations have proposed the occurrence of unusual softening of vibrational modes associated with internal vibrations of the IO_3 molecule. However, this hypothesis has not been confirmed by Raman experiments yet, which have been only reported at ambient conditions.[8,9]

Received: July 17, 2020
Revised: September 2, 2020
Published: September 11, 2020

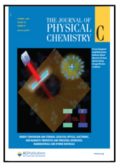

https://dx.doi.org/10.1021/acs.jpcc.0c06541
J. Phys. Chem. C 2020, 124, 21329−21337

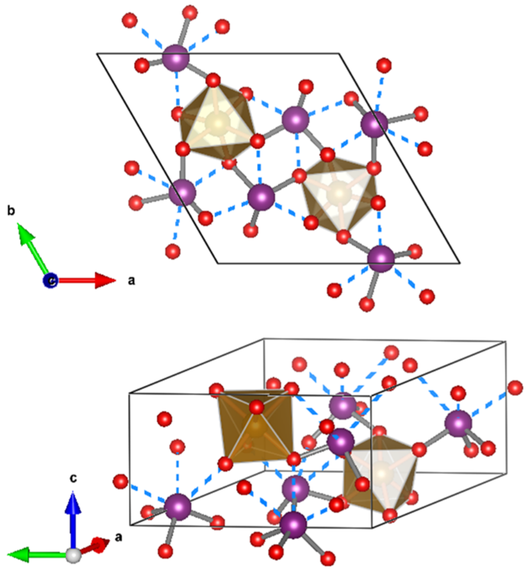

Figure 1. Schematic representation of the crystal structure of $Fe(IO_3)_3$ at room pressure. Two different perspectives are shown. FeO_6 octahedral units are shown in brown. I and O atoms are represented in purple and red, respectively. Short I−O bonds are shown with gray solid lines, while long I−O bonds that do not result in an increased coordination are shown with blue dashed lines. Fe atoms are sixfold coordinated, whereas I atoms are threefold coordinated.

In this work, we explore the proposed phonon-softening phenomenon by HP Raman spectroscopy (RS), which will be analyzed with the help of *ab initio* DFT calculations. We have performed HP RS experiments up to 21 GPa to minimize the influence of precursor effects of the first-order phase transition that has been reported to occur at 22 GPa. Combining experimental and theoretical results, we propose for the first time a tentative symmetry assignment for Raman modes of $Fe(IO_3)_3$ and discuss the nature of the soft phonons. In particular, we have found evidence of the occurrence of two subtle isostructural phase transitions (IPTs), which were not detected by previous studies.

Before presenting and discussing our results, we briefly describe the crystal structure of $Fe(IO_3)_3$, which is shown in Figure 1. The description of the structure is relevant for the discussion of the results reported here. In Figure 1, it can be seen that the structure is formed by FeO_6 octahedral units connected by isolated IO_3 trigonal pyramids which deviate from the ideal $3m$ point symmetry because the lone pair takes up a larger region of space than do the single I−O bonds. In the figure, we have included the bonds corresponding to the IO_3 coordination polyhedron and dashed lines indicating the three second-neighbor O atoms, which become relevant under compression.

We start discussing the Raman spectra under ambient conditions which are shown in Figure 2. The spectrum is very similar to those reported in the literature.[8,9] As can be observed, the Raman-active modes are distributed in two isolated regions. One region is for wavenumbers smaller than 500 cm^{-1} and the other is for wavenumbers larger than 650 cm^{-1}, with a phonon gap between the two regions. The strongest mode is located at 792 cm^{-1}. Along the paper, we show that the high-frequency modes are linked to I−O vibrations. In particular, they are internal modes of IO_3 units.

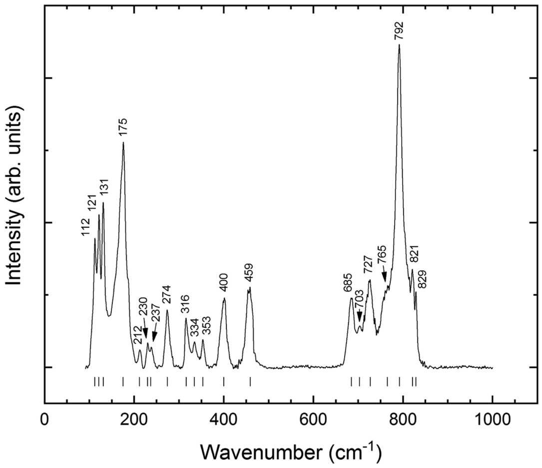

Figure 2. Ambient-pressure Raman spectrum of $Fe(IO_3)_3$ recorded outside the DAC. Ticks show the position of the identified modes. Their wavenumbers are also given.

For $Fe(IO_3)_3$, group theory predicts 37 Raman-active modes ($12A + 12E_1 + 13E_2$). In previous studies,[8,9] Ristic et al. measured 17 modes and Bushiri et al. measured 14 modes. In our experiments, we have measured 20 modes. The Raman-active modes are summarized in Table 1, where they have been given a superindex to number them in the order of increasing frequency. It can be seen that there is good agreement between the frequencies reported in different experiments.

DFT-calculated frequencies of $Fe(IO_3)_3$ are also listed in Table 1. DFT calculations give a good description of experimentally observed Raman-active mode frequencies, with the differences being smaller than 10%, which is typical for most oxides.[10] In particular, the mode frequencies of $Fe(IO_3)_3$ in the low-frequency region are slightly underestimated by our PBEsol + *U* calculations, as happens in many other oxides.[10] On the other hand, the calculated high-frequency modes have an offset of nearly 60 cm^{-1} with respect to experiments. The comparison of frequencies and their pressure dependences (to be discussed) allowed us to propose a tentative assignment of the experimentally observed Raman-active modes. The symmetry of the different modes is included in Table 1.

According to our mode assignment, the strongest Raman-active mode, located at a wavenumber of 792 cm^{-1} (A^{11} mode in Table 1), can be identified as an internal symmetric stretching vibration of O atoms against the I atom inside IO_3 units (see Figure S1 in the Supporting Information) and calculated to be at 729.2 cm^{-1} in Table 1. Notice that DFT describes properly not only Raman-active modes but also IR-active modes, which are already reported,[7] and their pressure dependence.

Interestingly, in many metal iodates with different compositions, the strongest Raman-active mode is always located in the 730−800 cm^{-1} region. In $Ni(IO_3)_2$, $Mn(IO_3)_2$, $Co(IO_3)_2$, and $Zn(IO_3)_2$, the strongest Raman-active mode is in the 763−782 cm^{-1} range.[11] In $Al(IO_3)_3$, $Ga(IO_3)_3$, and $In(IO_3)_3$, it is in the 730−800 cm^{-1} range.[12] Finally, in KIO_3, the strongest mode[13] is at 748 cm^{-1}. All these iodates have in common that in their structure, iodine atoms form IO_3 trigonal pyramids with very short I−O bond distances. Based on this fact, it has been generally assumed that the strongest Raman-active mode of each compound is an internal symmetric stretching I−O vibration inside the IO_3 unit. In the case of

Table 1. Theoretical and Experimental Zero-Pressure Frequencies, ω, Pressure Coefficients, dω/dP, and Grüneisen Parameters, γ, of Raman-Active Modes of $Fe(IO_3)_3$[a]

	theory			experiment				
mode	ω_0[b] (cm^{-1})	dω/dP[b] (cm^{-1}/GPa)	γ[b]	ω_0[b] (cm^{-1})	dω/dP[b] (cm^{-1}/GPa)	γ[b]	ω_0[c] (cm^{-1})	ω_0[d] (cm^{-1})
A^1(RI)	57.3	−0.08	−0.05					55
E_1^1(RI)	65.6	3.10	1.70					
E_2^1(R)	79.8	1.24	0.56					
E_2^2(R)	89.6	5.21	2.09				86	85
A^2(RI)	112.3	4.88	1.56	112	2.44	1.20		110
E_1^2(RI)	119.8	2.48	0.75	121	1.78	0.81	125	125
A^3(RI)	126.1	1.85	0.53					
E_2^3(R)	131.8	5.57	1.52	131	3.57	1.50		
E_1^3(RI)	165.4	3.96	0.86	175	0.70	0.22	166	165
E_2^4(R)	172.3	6.65	1.39					
E_2^5(R)	194.5	4.49	0.83					
E_1^4(RI)	202.2	6.16	1.10					
A^4(RI)	212.7	2.53	0.43	212	2.76	0.72		205
E_1^5(RI)	219.4	9.30	1.53					
E_2^6(R)	223.5	5.17	0.83	230	4.27	1.02	223	225
A^5(RI)	239.8	6.48	0.97	237	6.76	1.57		
E_2^7(R)	245.3	7.99	1.17					
E_1^6(RI)	269.8	4.83	0.64					
A^6(RI)	270.7	7.35	0.98	274	7.14	1.43	266	265
A^7(RI)	291.7	1.88	0.23	316	0.65	0.11	320	315
E_1^7(RI)	316.5	4.51	0.51	334	1.36	0.22		
E_2^8(R)	334.2	2.90	0.31	353	1.78	0.28	350	350
E_1^8(RI)	382.5	4.06	0.38					
E_2^9(R)	385.5	6.06	0.57					
A^8(RI)	391.4	3.02	0.28	400	4.27	0.59	394	395
A^9(RI)	436.9	7.89	0.65	459	5.78	0.69	450	445
E_2^{10}(R)	445.1	7.15	0.58					
E_1^9(RI)	445.9	7.74	0.62					
E_2^{11}(R)	619.8	−1.40	−0.08					
E_1^{10}(RI)	622.1	−0.65	−0.04	685	−0.20	−0.02	685	685
A^{10}(RI)	637.7	−1.68	−0.09	703	−2.32	−0.18		
E_2^{12}(R)	674.7	0.07	0.00	727	−0.87	−0.07	726	726
E_1^{11}(RI)	697.9	−2.38	−0.12	765	−3.72	−0.27	755	756
A^{11}(RI)	729.2	−1.45	−0.07	792	−3.51	−0.24	795	796
E_1^{12}(RI)	770.7	−5.59	−0.26	821	−3.40	−0.23		826
A^{12}(RI)	774.0	−6.95	−0.32	829	−6.41	−0.43	831	
E_2^{13}(R)	791.1	−5.25	−0.24					

[a] In fact, our experimental frequencies correspond to 0.5 GPa. Raman-active (R) or both Raman- and IR-active (RI) are indicated. Results of previous experiments[8,9] have also been included for comparison. To calculate the Grüneisen parameters, we have used the theoretical bulk modulus (36 GPa) for calculations and the experimental bulk modulus (55 GPa) for experiments.[7] [b] This work. [c] Ref.[9] [d] Ref.[8]

$Fe(IO_3)_3$, we support this conclusion by calculating the atomic motions associated with these modes (see Figure S1). This fact will be discussed in more detail when presenting the HP results. The three Raman-active modes (E_1^{12}, A^{12}, and E_2^{13}) with higher frequencies than the symmetric stretching mode correspond to asymmetric stretching I−O vibrations inside the IO_3 unit (see Figures S2−S4 in the Supporting Information).

We now start discussing the HP behavior of the Raman spectra in $Fe(IO_3)_3$. In Figure 3, we show Raman spectra at different pressures. In Figure 4, we show the pressure dependence of phonon wavenumbers. The spectrum measured at 0.5 GPa is very similar to the ambient-pressure spectrum shown in Figure 2. The Raman spectra under compression show a monotonous behavior with no abrupt frequency changes up to 21 GPa, indicating that a first-order transition does not happen in this pressure range. The intensity changes observed beyond 15 GPa for the modes around 150 and 320 cm^{-1} are related to phonon merging or splitting due to the different pressure dependences of modes (see Figure 4). The nonoccurrence of a first-order transition in the pressure range of the present study is in good agreement with the results from previous XRD measurements.[7] Previous IR spectroscopy studies located the transition at 15 GPa.[7] The lower transition pressure observed in these experiments is due to the use of a less hydrostatic medium in IR experiments (CsI) than in present Raman and previous XRD experiments (silicone oil).[7,10,14,15] However, when analyzing the pressure dependence of modes with the help of DFT calculations, we have found that there are modes showing strong nonlinear pressure dependences and soft-mode behaviors (see Figure 4) that suggest possible continuous transitions as discussed next. All changes observed in the RS spectrum under compression are reversible, as can be seen in Figure 3 in the top RS spectrum

https://dx.doi.org/10.1021/acs.jpcc.0c06541
J. Phys. Chem. C 2020, 124, 21329−21337

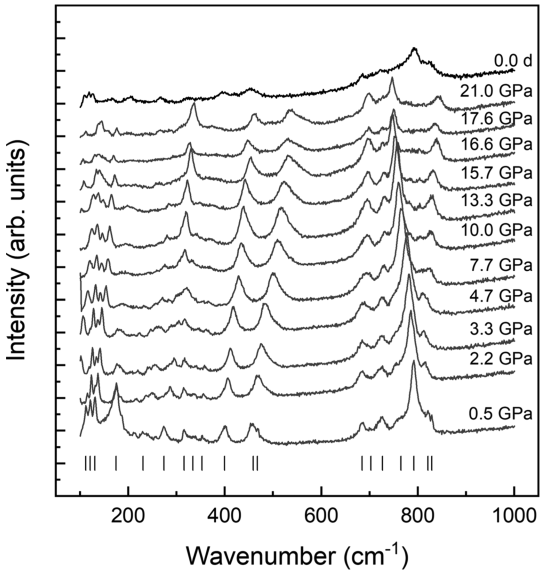

Figure 3. Selection of Raman spectra recorded in $Fe(IO_3)_3$ at different pressures. The top Raman spectrum was taken upon decompression "d" to show the reversibility of the process. Bottom marks indicate the frequencies of the experimental modes at the smallest pressure.

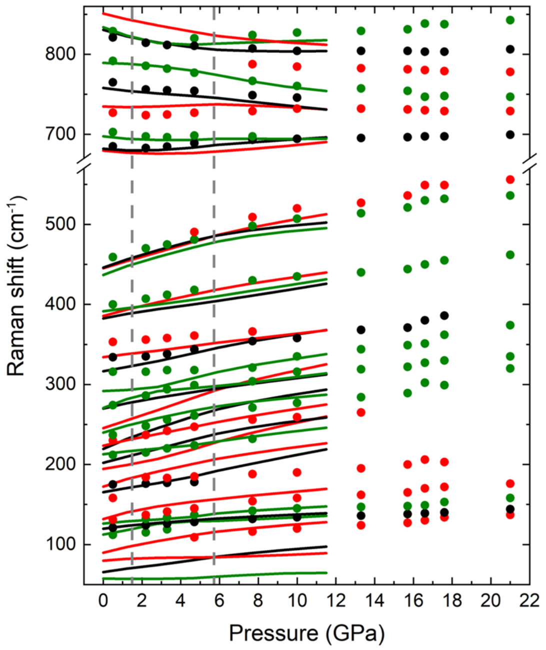

Figure 4. Experimental (symbols) and theoretical (solid lines) pressure dependence of Raman-active mode frequencies in $Fe(IO_3)_3$. The green, black, and red colors correspond to the A, E_1, and E_2 modes, respectively. In the high-frequency region (top panel), calculated modes have been shifted 60 cm^{-1} to higher frequencies to facilitate comparison with experiments. The vertical dashed lines indicate the pressures where changes associated to the two IPTs can be observed.

recorded after decompression. Note that at 10 GPa, there are two peaks near 300 cm^{-1} that overlap. This causes an apparent increase in intensity at this frequency. In Figure 3, a pressure-induced closing of the phonon gap can be also noticed. This fact is mainly caused by the hardening of modes below 450 cm^{-1} and the softening of all the measured high-frequency modes. Therefore, the closing of the phonon gap, more evident in Figure 4, where we have plotted the pressure dependence of the experimental and theoretical Raman-active modes, also suggests an increase of I coordination.

Experimental and theoretical zero-pressure frequencies, pressure coefficients, and Grüneissen parameters show relatively good agreement, as can be seen in Figure 4 and in Table 1. In the figure, DFT results are shown only up to 12 GPa because they underestimate the transition pressure of the first-order transition, as discussed in ref 7. Therefore, for consistency, DFT results are compared with experiments only for the pressures below the theoretical first-order phase transition. As observed in Figure 4, many Raman-active modes show anomalous pressure dependences. Not only there are high-frequency soft modes but also there are many modes in the low- and high-frequency regions that show an S-like nonlinear pressure dependence that will be commented later. Consequently, the zero-pressure coefficients in Table 1 have been obtained using the pressure range where the frequency dependence is linear with pressure, near 0 GPa, and the Grüneisen parameters have been calculated using the bulk moduli given in the caption of Table 1. In Figures 3 and 4, it can be seen that there is a progressive closing of the phonon gap with increasing pressure, which suggests the existence of a close first-order phase transition above 21 GPa, that is, consistent with XRD measurements.[7] Additionally, in the high-frequency region, all the modes of $Fe(IO_3)_3$ have a soft-mode behavior, at least between 0 and 2 GPa. Using J-ICE, we have identified that the high-frequency modes mainly correspond to symmetric and asymmetric I—O stretching vibrations inside the IO_3 units (see Figures S1−S4 for examples). As shown in Figure 4, DFT not only supports the existence of soft modes but also provides a qualitatively good description for the pressure dependence of most observed modes. Note that for high-frequency modes, theoretical calculations describe nicely the pressure dependence of experimental mode frequencies when an upward shift of 60 cm^{-1} is applied to calculated frequencies.

Interestingly, we have found that one of the experimental soft modes of $Fe(IO_3)_3$ is the strongest mode at 792 cm^{-1} that we have tentatively attributed to the A^{11} mode (with a calculated frequency of 729.2 cm^{-1}). The observed mode softening of the high-frequency modes can be correlated to the pressure-induced increase of two of the short I—O bond distances (see Figure 5), which is expected to reduce the restoring force of stretching vibrations. According to our calculations, iodine atoms are threefold coordinated at room pressure. However, by considering as coordinated to iodine all those oxygen atoms with an I—O bond length up to 33% larger than the maximum distance among the three short I—O bonds, it can be concluded that the coordination number of iodine increases as pressure increases. In particular, the iodine coordination first becomes fourfold (at least above 5.7 GPa) and then gradually approaches a sixfold coordination (see Figure 5), becoming six at the phase transition at 22 GPa.[7] This can be explained by the progressive reduction of the iodine LEP stereoactivity with increasing pressure, as found in a number of heavy pnictogen (As, Sb, and Bi) compounds with a strong LEP stereoactivity at room pressure, such as α-Sb_2O_3,[16−18] β-Bi_2O_3,[19,20] isostructural Sb_2S_3, Sb_2Se_3, and Bi_2S_3 compounds,[21] α-As_2Te_3,[22] $SbPO_4$,[23] and As_2S_3.[24]

Under a harmonic approximation, it can be assumed as a first approximation that the force constant, *k*, of the internal

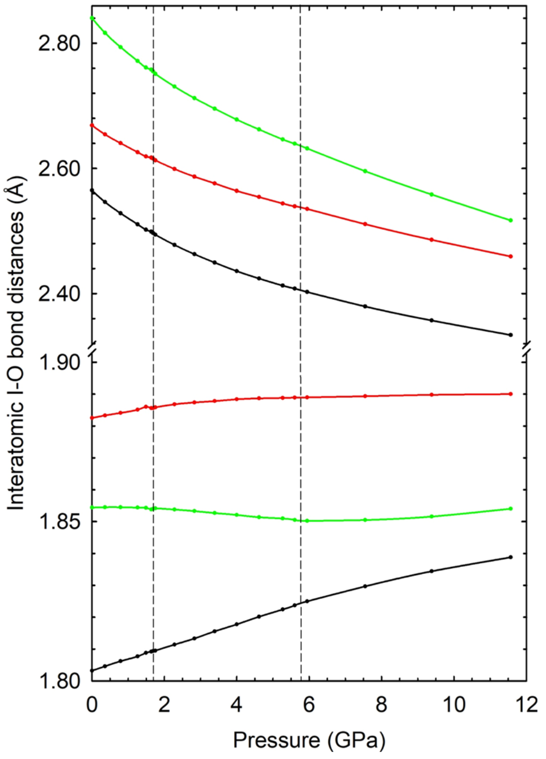

Figure 5. Calculated pressure dependence of I−O bond distances. The vertical dashed lines indicate the pressures where changes associated to the two IPTs can be observed. A gradual increase of I coordination can be inferred from this figure.

phonons of IO_3 is a function of $(d_{I-O})^{-3}$, where d_{I-O} is the average I−O bond distance.[25] Because the frequency of a stretching mode is proportional to the square root of the force constant and inversely proportional to the square root of the reduced mass, μ, of the bond, $\omega = (k/\mu)^{1/2}$, we have that $\omega^{-2/3}$ should have a linear dependence on the average I−O bond distance. Using the results of our calculations, we have correlated the theoretical frequencies of the soft modes with the theoretical average I−O bond distance in IO_3 units (see Figure 6). Here, it can be seen that indeed there is a clear linear relationship between the $\omega^{-2/3}$ and the calculated average I−O bond distance for the soft high-frequency modes. Thus, the decrease of the phonon frequencies is a consequence of the slight enlargement of the three shortest I−O distances in order to accommodate additional O atoms around iodine as pressure increases.

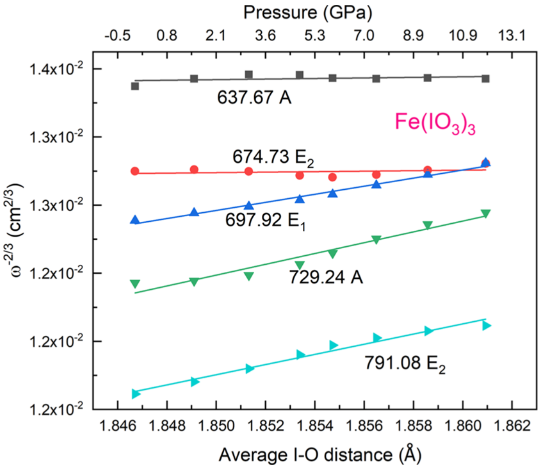

Figure 6. Theoretical $\omega^{-2/3}$ vs average theoretical I−O bond distances in IO_3 units of $Fe(IO_3)_3$. In the upper axis, the pressure of each average bond distance is indicated. It can be seen that the average I−O bond distance increases under compression.

It is noteworthy that the average distance of the three short I−O bonds of the IO_3 unit increases slightly under compression because of the changes induced by pressure in the crystal structure of $Fe(IO_3)_3$.[7] Simultaneously, second-neighbor I−O distances above 2.5 Å show a notable decrease at HP (see Figure 5). Therefore, these O atoms enter progressively into the coordination sphere of iodine atoms and induce changes in the coordination of I atoms. We believe that the enlargement of the short I−O bonds under compression is responsible for the softening of most high-frequency modes and is a consequence of a charge transfer from the short I−O bonds to the large I−O bonds in order to increase the iodine coordination. Such an increase of the bond distance and decrease of the bond charge has been recently observed in As_2S_3[24] and has been related to the novel phenomena of "metavalent" bonding, that is, the observation of a new type of chemical bonding intermediate between covalent and metallic bonding and characterized by bonds with less than two electrons per bond.[26,27] In some oxides with strong LEP stereoactivity at room pressure, this behavior has been related to the existence of unusual IPTs, such as in α-Sb_2O_3[16−18] and β-Bi_2O_3.[19,20]

We now present evidence supporting the existence of subtle IPTs in $Fe(IO_3)_3$. Such transitions were not detected by previous XRD studies because these subtle phase transitions involve only continuous changes in the crystal structure, with no discontinuities in the unit-cell parameters or atomic positions. In contrast, RS experiments, sensing local properties, as the vibrations are, are more sensitive for detecting such subtle transitions. We have found evidence for the two IPTs not only from the pressure dependence of phonons and bond distances but also from the analysis of atomic positions and elastic constants that correlate with changes in lattice parameters at HP. A detailed analysis of all this information places the transitions, near 1.5−2.0 and 5.7−6.0 GPa. For the sake of briefness, we present the evidence for the two IPTs in Figures S5−S10 of the Supporting Information. These figures show the theoretical pressure dependence of the unit-cell parameters and free atomic parameters of $Fe(IO_3)_3$. In particular, the two IPTs, marked by the vertical dashed lines in these figures, can explain the strong nonlinear S-like behavior of a number of parameters of $Fe(IO_3)_3$; for instance, the z-coordinate of the Fe atom. Additional support for the two IPTs near 1.5 and 5.7 GPa comes from the pressure dependence of the elastic constants, which is shown in Figure 7. In particular, at 1.7 GPa, there is a clear jump of C_{33}, C_{66}, C_{12}, and C_{13}. Such changes are indicative of the occurrence of phase transitions.[28−30] At 5.7 GPa, there are also changes in the elastic constant, and they are less evident than at 1.7 GPa; however, there are detectable changes in the pressure dependence of C_{13} and C_{33}, as can be seen in Figure 7.

In order to understand the nature of the two IPTs without change of volume, we have calculated the phonon dispersion curves of $Fe(IO_3)_3$ at 0, 1.5, 5.7, and 7.5 GPa, which are shown in Figure 8. As observed, the phonon dispersion curves show small dynamic instabilities (negative frequencies) near the Γ-point at 1.5 and 5.7 GPa that are not observed either at 0 GPa

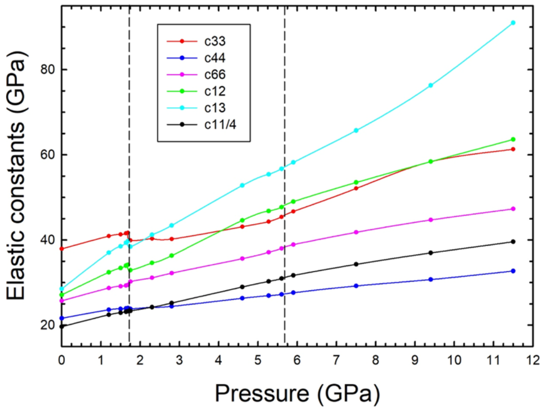

Figure 7. Calculated pressure dependence of elastic constants in $Fe(IO_3)_3$. The vertical dashed lines indicate the pressures where changes due to the two IPTs can be observed. Note the changes of the elastic constants especially around 1.5 GPa.

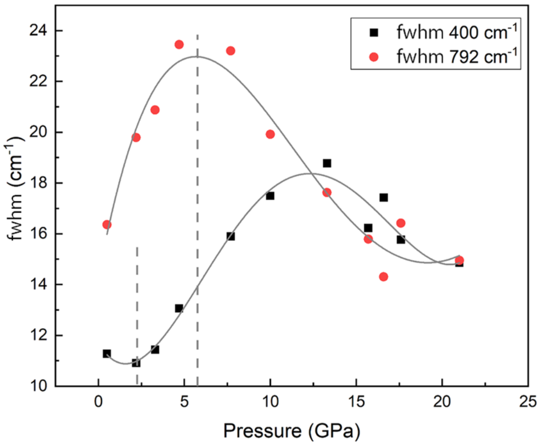

Figure 9. Pressure dependence of the fwhm of phonons with wavenumbers of 400 and 792 cm^{-1}.

or at 7.5 GPa. Consequently, we can conclude that the two IPTs observed in $Fe(IO_3)_3$ are of similar nature to the one of tetragonal β-Bi_2O_3[19,20] and perhaps also in α-Sb_2O_3.[16−18]

Additional support to the existence of two IPTs in $Fe(IO_3)_3$ comes from the study of phonon lifetime change with pressure. In the case of RS, the full width at half-maximum (fwhm) is related inversely to the phonon lifetime. The pressure dependence of the fwhm of two modes of $Fe(IO_3)_3$, which do not overlap with other modes, is shown in Figure 9. It is evident from the figure that the line width of the mode with a wavenumber of 400 cm^{-1} increases substantially with pressure beyond 2 GPa. On the other hand, the mode with a wavenumber of 792 cm^{-1} has a sharp change in the pressure evolution of the line width at 6 GPa. Such changes are typical of IPT transitions.[18−22] We think that the fact that they take place at the same pressure that changes in pressure dependence of phonons, bond distances, and elastic constants is not a mere coincidence but another evidence of the occurrence of IPTs in $Fe(IO_3)_3$. Additional changes are observed in the behavior of phonon fwhm around 15−20 GPa, but they are related to precursor effects of the first-order transition previously reported at 22 GPa.

Summing up, both Raman experiments and DFT calculations support that there are soft modes in $Fe(IO_3)_3$ which are related to the increase of the three short I−O bonds with pressure. The short I−O bonds increase, while the second-neighbor I−O bonds decrease with pressure. Moreover, the nonlinear S-like behavior of several Raman-active modes (also of several IR-active modes)[7] as well as of some elastic

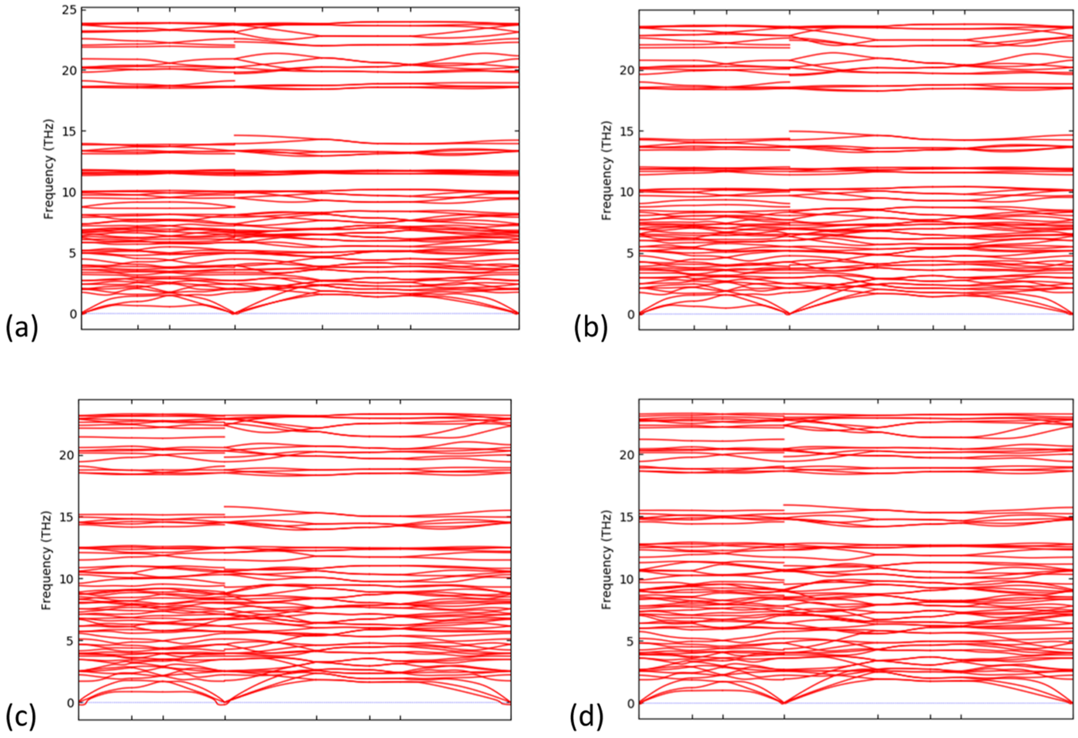

Figure 8. Calculated phonon dispersion curves along the Γ−*M*−*K*−Γ−*A*−*L*−*H*−Γ direction at 0 (a), 1.5 (b), 5.7 (c), and 7.5 GPa (d). At 1.5 and 5.7 GPa, small dynamic instabilities (smaller at 1.5 GPa) are observed near the Γ-point which are not observed at 0 and 7.5 GPa.

constants can be explained by the occurrence of two IPTs around 1.5−2.0 and 5.7−6.0 GPa. The two IPTs are clearly related to changes in the behavior of lattice parameters and free atomic positions.

The formation of additional I−O bonds at HP in metal iodates has important consequences of the behavior of phonons under compression.[31] Therefore, the present discovery of continuous IPTs in a metal iodate, such as $Fe(IO_3)_3$, opens the door to interesting findings in this family of compounds at HP. In particular, we have noticed that in KIO_3 also, two internal stretching modes of the IO_3 unit are soft modes.[13] This compound undergoes a phase transition at 5 GPa. It would be not surprising that the observed soft modes in KIO_3 could be related to a collective instability which makes the crystal structure unstable, thus triggering a phase transition.[32,33] This suggests that the triggering of phase transitions by soft modes could be a common feature of metal iodates.

In conclusion, the lattice dynamics of $Fe(IO_3)_3$ has been studied up to 21 GPa, within the range of stability of the low-pressure hexagonal phase, by means of RS measurements, which have been interpreted using DFT calculations. Our measurements and calculations evidence a progressive decrease of the phonon gap and the softening of most high-frequency vibrational modes at least up to 2 GPa. The frequency, pressure dependence, and symmetry of the different modes have been determined. The soft modes in the high-frequency region are related to internal I−O vibrations of IO_3 units. Among them, we include the symmetric stretching I−O vibration of IO_3 units, which is the strongest Raman-active mode. The soft mode behavior is proposed to be connected with the increase of the shortest I−O bond distances because of a gradual increase of the iodine coordination that leads to a decrease of the short I−O bond forces due to a charge transfer to long I−O distances. The nonlinear S-like behavior of a number of experimental and theoretical Raman-active modes, as well as other physical properties, can be explained by the existence of two IPTs at 1.5−2.0 and 5.7−6.0 GPa which occur without a volume change and only a change in volume compressibility. Our results have been compared with the results from other metal iodates in order to try to find general features in the iodate family. The present discovery of unusual IPTs in a metal iodate, such as $Fe(IO_3)_3$, and their relationship to soft modes open the door to interesting findings in the iodate family of compounds under compression and invite to revisit the HP behavior of iodine-based compounds, such as KIO_3.

■ METHODS

Samples. For the study of $Fe(IO_3)_3$, we used the same sample used in our previous XRD and IR studies[7] that was prepared by a coprecipitation technique. A description of the sample preparation method can be found in ref 7. The purity of the sample and crystal structure were confirmed by XRD measurements.[7]

HP Generation. We performed HP RS measurements at room temperature up to 21 GPa using silicone oil as a pressure-transmitting medium (PTM)[14,15] to avoid the hydration of the metal iodates[1] and the ruby fluorescence scale as our pressure gauge.[34] The silicone fluid is as good a PTM as a 4:1 methanol/ethanol mixture up to a pressure of about 20 GPa.[35] For these studies, samples, ruby chips, and the PTM were loaded in the 200 μm diameter hole of a preindented steel gasket inside a diamond-anvil cell (DAC). We made a careful loading of materials inside the DAC to avoid both sample hydration and sample bridging between diamond anvils.[36] Because of the size of the ruby pressure gauge and the distance between ruby chips and the measuring point (sample position), there is a radial pressure inhomogeneity in the DAC. We estimate the pressure difference between ruby and the sample to be smaller than 3% of the ruby pressure.[37]

Raman Spectroscopy. HP RS measurements, with a fixed time of 20 s, were performed using an inVia Renishaw Raman spectrometer system with a 5× magnification objective. A laser wavelength of 532 nm and a grating of 2400 lines·mm^{-1} provided a spectral resolution better than 2 cm^{-1}. A laser power inferior to 10 mW before the DAC was used to avoid sample heating.

Overview of the Calculations. DFT calculations were used for the interpretation of experiments and mode assignment. Total-energy and phonon calculations as a function of pressure for $Fe(IO_3)_3$ were previously published by a part of the coauthors of this work.[7] Such calculations were performed using the Vienna Ab initio Simulation Package (VASP) within the generalized gradient approximation with the Perdew−Burke−Ernzerhof (PBE) for solids (PBEsol) functionals. The Hubbard potential, U, was also used (U_{eff} = 5.4 eV) to account for the strong correlation between the electrons in the d shell, as previously performed to explain XRD and IR results.[7] After optimizing the crystal structure at different pressures, the phonon frequencies and phonon dispersion curves were calculated using the direct force method. The elastic constants were calculated using density functional perturbation theory. Thanks to DFT calculations, we have been able to identify atomic motions associated with phonons using the J-ICE software.[38]

■ ASSOCIATED CONTENT

Supporting Information

The Supporting Information is available free of charge at https://pubs.acs.org/doi/10.1021/acs.jpcc.0c06541.

Atomic vibrations of Raman modes and calculated pressure dependence of unit-cell parameters and atomic positions (PDF)

■ AUTHOR INFORMATION

Corresponding Author

Daniel Errandonea − *Departamento de Física Aplicada—ICMUV—MALTA Consolider Team, Universitat de València, 46100 Burjassot, Valencia, Spain;* orcid.org/0000-0003-0189-4221; Email: daniel.errandonea@uv.es

Authors

Akun Liang − *Departamento de Física Aplicada—ICMUV—MALTA Consolider Team, Universitat de València, 46100 Burjassot, Valencia, Spain*
Saqib Rahman − *Center for High Pressure Science and Technology Advanced Research, 201203 Shanghai, China*
Placida Rodriguez-Hernandez − *Departamento Física, Malta Consolider Team, and Instituto de Materiales y Nanotecnología, Universidad de La Laguna, 38206 La Laguna, Tenerife, Spain;* orcid.org/0000-0002-4148-6516
Alfonso Muñoz − *Departamento Física, Malta Consolider Team, and Instituto de Materiales y Nanotecnología,*

Universidad de La Laguna, 38206 La Laguna, Tenerife, Spain; orcid.org/0000-0003-3347-6518

Francisco Javier Manjón − *Instituto de Diseño para la Fabricación y Producción Automatizada, MALTA-Consolider Team, Universitat Politècnica de València, 46022 Valencia, Spain;* orcid.org/0000-0002-3926-1705

Gwilherm Nenert − *Malvern Panalytical B.V., 7602 EA Almelo, The Netherlands*

Complete contact information is available at: https://pubs.acs.org/10.1021/acs.jpcc.0c06541

Author Contributions

The manuscript was written through contributions of all authors. All authors have given approval to the final version of the manuscript.

Notes

The authors declare no competing financial interest.

■ ACKNOWLEDGMENTS

This work was supported by the Spanish Ministry of Science, Innovation and Universities, the Spanish Research Agency (AEI), the European Fund for Regional Development (ERDF, FEDER) under grants MAT2016-75586-C4-1/2/3-P, PID2019-106383GB-C41/42/43, and RED2018-102612-T (MALTA Consolider-Team Network), and the Generalitat Valenciana under grant Prometeo/2018/123 (EFIMAT). A.L. and D.E. would like to thank the Generalitat Valenciana for the Ph.D. fellowship GRISOLIAP/2019/025).

■ REFERENCES

(1) Nassau, K.; Shiever, J. W.; Prescott, B. E. Transition Metal Iodates. I. Preparation and Characterization of the 3d Iodates. *J. Solid State Chem.* **1973**, *7*, 186−204.

(2) Jansen, M. Zur Kistallstruktur von FeJ_3O_9. *J. Solid State Chem.* **1976**, *17*, 1−6.

(3) Hu, C.-L.; Mao, J.-G. Recent Advances on Second-Order NLO Materials Based on Metal Iodates. *Coord. Chem. Rev.* **2015**, *288*, 1−17.

(4) Hebboul, Z.; Galez, C.; Benbertal, D.; Beauquis, S.; Mugnier, Y.; Benmakhlouf, A.; Bouchenafa, M.; Errandonea, D. Synthesis, Characterization, and Crystal Structure Determination of a New Lithium Zinc Iodate Polymorph LiZn(IO$_3$)$_3$. *Crystals* **2019**, *9*, 464.

(5) Bergman, J. G.; Boyd, G. D.; Ashkin, A.; Kurtz, S. K. New Nonlinear Optical Materials: Metal Oxides with Nonbonded Electrons. *J. Appl. Phys.* **1969**, *40*, 2860−2863.

(6) Sagotra, A. K.; Errandonea, D.; Cazorla, C. Mechanocaloric Effects in Superionic Thin Films from Atomistic Simulations. *Nat. Commun.* **2017**, *8*, 963.

(7) Liang, A.; Rahman, S.; Saqib, H.; Rodriguez-Hernandez, P.; Muñoz, A.; Nénert, G.; Yousef, I.; Popescu, C.; Errandonea, D. First-Order Isostructural Phase Transition Induced by High-Pressure in Fe(IO 3) 3. *J. Phys. Chem. C* **2020**, *124*, 8669−8679.

(8) Ristić, M.; Musić, S.; Ivanda, M. A Study of the Thermal Stability of Fe(IO$_3$)$_3$ by ^{57}Fe Mossbauer, FT- IR and Raman Spectroscopies. *J. Mol. Struct.* **1999**, *480*−*481*, 637−640.

(9) Bushiri, M. J.; Kochuthresia, T. C.; Vaidyan, V. K.; Gautier-Luneau, I. Raman Scattering Structural Studies of Nonlinear Optical M(IO$_3$)$_3$(M=Fe, Ga, α-In) and Linear Optical β-In(IO$_3$)$_3$. *J. Nonlinear Opt. Phys. Mater.* **2014**, *23*, 1450039.

(10) Errandonea, D.; Muñoz, A.; Rodríguez-Hernández, P.; Gomis, O.; Achary, S. N.; Popescu, C.; Patwe, S. J.; Tyagi, A. K. High-Pressure Crystal Structure, Lattice Vibrations, and Band Structure of BiSbO$_4$. *Inorg. Chem.* **2016**, *55*, 4958−4969.

(11) Kochuthresia, T. C.; Gautier-Luneau, I.; Vaidyan, V. K.; Bushiri, M. J. Raman and Ftir Spectral Investigations of Twinned M(IO$_3$)$_2$ (M = Mn, Ni, Co, AND Zn) Crystals. *J. Appl. Spectrosc.* **2016**, *82*, 941−946.

(12) Ngo, N.; Kalachnikova, K.; Assefa, Z.; Haire, R. G.; Sykora, R. E. Synthesis and Structure of In(IO3)3 and Vibrational Spectroscopy of M(IO3)$_3$ (M=Al, Ga, In). *J. Solid State Chem.* **2006**, *179*, 3824−3830.

(13) Shen, Z. X.; Wang, X. B.; Li, H. P.; Tang, S. H.; Zhou, F. High Pressure Raman Study and Phase Transitions of KIO$_3$ Non-Linear Optical Single Crystals. *Rev. High Pressure Sci. Technol.* **1998**, *7*, 751−753.

(14) Klotz, S.; Chervin, J.-C.; Munsch, P.; Le Marchand, G. Hydrostatic Limits of 11 Pressure Transmitting Media. *J. Phys. D: Appl. Phys.* **2009**, *42*, 075413.

(15) Errandonea, D.; Meng, Y.; Somayazulu, M.; Häusermann, D. Pressure-Induced → ω Transition in Titanium Metal: A Systematic Study of the Effects of Uniaxial Stress. *Phys. B* **2005**, *355*, 116−125.

(16) Sui, Z.; Hu, S.; Chen, H.; Gao, C.; Su, H.; Rahman, A.; Dai, R.; Wang, Z.; Zheng, X.; Zhang, Z. Laser Effects on Phase Transition for Cubic Sb$_2$O$_3$ Microcrystals under High Pressure. *J. Mater. Chem. C* **2017**, *5*, 5451−5457.

(17) Zhao, Z.; Zeng, Q.; Zhang, H.; Wang, S.; Hirai, S.; Zeng, Z.; Mao, W. L. Structural Transition and Amorphization in Compressed α-Sb$_2$O$_3$. *Phys. Rev. B: Condens. Matter Mater. Phys.* **2015**, *91*, 184112.

(18) Pereira, A. L. J.; Gracia, L.; Santamaría-Pérez, D.; Vilaplana, R.; Manjón, F. J.; Errandonea, D.; Nalin, M.; Beltrán, A. Structural and Vibrational Study of Cubic Sb$_2$O$_3$ under High Pressure. *Phys. Rev. B: Condens. Matter Mater. Phys.* **2012**, *85*, 174108.

(19) Pereira, A. L. J.; Gomis, O.; Sans, J. A.; Contreras-García, J.; Manjón, F. J.; Rodríguez-Hernández, P.; Muñoz, A.; Beltrán, A. β-Bi$_2$O$_3$ under Compression: Optical and Elastic Properties and Electron Density Topology Analysis. *Phys. Rev. B* **2016**, *93*, 224111.

(20) Pereira, A. L. J.; Sans, J. A.; Vilaplana, R.; Gomis, O.; Manjón, F. J.; Rodríguez-Hernández, P.; Muñoz, A.; Popescu, C.; Beltrán, A. Isostructural Second-Order Phase Transition of β-Bi$_2$O$_3$ at High Pressures: An Experimental and Theoretical Study. *J. Phys. Chem. C* **2014**, *118*, 23189−23201.

(21) Ibáñez, J.; Sans, J. A.; Popescu, C.; López-Vidrier, J.; Elvira-Betanzos, J. J.; Cuenca-Gotor, V. P.; Gomis, O.; Manjón, F. J.; Rodríguez-Hernández, P.; Muñoz, A. Structural, Vibrational, and Electronic Study of Sb$_2$S$_3$ at High Pressure. *J. Phys. Chem. C* **2016**, *120*, 10547−10558.

(22) Cuenca-Gotor, V. P.; Sans, J. A.; Ibáñez, J.; Popescu, C.; Gomis, O.; Vilaplana, R.; Manjón, F. J.; Leonardo, A.; Sagasta, E.; Suárez-Alcubilla, A.; et al. Structural, Vibrational, and Electronic Study of α-As$_2$Te$_3$ under Compression. *J. Phys. Chem. C* **2016**, *120*, 19340−19352.

(23) Pereira, A. L. D. J.; Santamaría-Pérez, D.; Vilaplana, R.; Errandonea, D.; Popescu, C.; Da Silva, E. L.; Sans, J. A.; Rodríguez-Carvajal, J.; Muñoz, A.; Rodríguez-Hernández, P.; et al. Experimental and Theoretical Study of SbPO$_4$ under Compression. *Inorg. Chem.* **2020**, *59*, 287−307.

(24) Cuenca-Gotor, V. P.; Sans, J. Á.; Gomis, O.; Mujica, A.; Radescu, S.; Muñoz, A.; Rodríguez-Hernández, P.; Da Silva, E. L.; Popescu, C.; Ibañez, J.; et al. Orpiment under Compression: Metavalent Bonding at High Pressure. *Phys. Chem. Chem. Phys.* **2020**, *22*, 3352−3369.

(25) Bucknum, M. J. Chemical Physics of Phonons and Superconductivity: A Heuristic Approach. *Nat. Preced.* **2008**, *1586*, 2.

(26) Wuttig, M.; Deringer, V. L.; Gonze, X.; Bichara, C.; Raty, J.-Y. Incipient Metals: Functional Materials with a Unique Bonding Mechanism. *Adv. Mater.* **2018**, *30*, 1803777.

(27) Raty, J. Y.; Schumacher, M.; Golub, P.; Deringer, V. L.; Gatti, C.; Wuttig, M. A Quantum-Mechanical Map for Bonding and Properties in Solids. *Adv. Mater.* **2019**, *31*, 1806280.

(28) Boccara, N. Second-Order Phase Transitions Characterized by a Deformation of the Unit Cell. *Ann. Phys.* **1968**, *47*, 40−64.

(29) Errandonea, D. Landau Theory Applied to Phase Transitions in Calcium Orthotungstate and Isostructural Compounds. *Europhys. Lett.* **2007**, *77*, 56001.

(30) Tröster, A.; Schranz, W.; Ehsan, S.; Belbase, K.; Blaha, P. Symmetry-Adapted Finite Strain Landau Theory Applied to $KMnF_3$. *Crystals* **2020**, *10*, 124.

(31) Monteseguro, V.; Errandonea, D.; Achary, S. N.; Sans, J. A.; Manjón, F. J.; Gallego-Parra, S.; Popescu, C. Structural Characterization of Aurophilic Gold(I) Iodide under High Pressure. *Inorg. Chem.* **2019**, *58*, 10665−10670.

(32) Errandonea, D.; Pellicer-Porres, J.; Pujol, M. C.; Carvajal, J. J.; Aguiló, M. Room-Temperature Vibrational Properties of Potassium Gadolinium Double Tungstate under Compression up to 32 GPa. *J. Alloys Compd.* **2015**, *638*, 14−20.

(33) Liu, J.; Shen, Z.; Zhang, Y.; Yin, X.; He, S. The P-T Phase Diagram of Lithium Iodate ($LiIO_3$) up to 40 Kbars. *Acta Phys. Sin.* **1983**, *32*, 118−123.

(34) Mao, H. K.; Xu, J.; Bell, P. M. Calibration of the Ruby Pressure Gauge to 800 Kbar under Quasi-Hydrostatic Conditions. *J. Geophys. Res.* **1986**, *91*, 4673−4676.

(35) Shen, Y.; Kumar, R. S.; Pravica, M.; Nicol, M. F. Characteristics of silicone fluid as a pressure transmitting medium in diamond anvil cells. *Rev. Sci. Instrum.* **2004**, *75*, 4450−4454.

(36) Errandonea, D.; Muñoz, A.; Gonzalez-Platas, J. Comment on High-Pressure x-Ray Diffraction Study of YBO_3/Eu^{3+}, $GdBO_3$, and $EuBO_3$: Pressure-Induced Amorphization in $GdBO_3$. *J. Appl. Phys.* **2014**, *115*, 216101.

(37) Jayaraman, A. Diamond anvil cell and high-pressure physical investigations. *Rev. Mod. Phys.* **1983**, *55*, 65−108.

(38) Canepa, P.; Hanson, R. M.; Ugliengo, P.; Alfredsson, M. J-ICE: A New Jmol Interface for Handling and Visualizing Crystallographic and Electronic Properties. *J. Appl. Crystallogr.* **2011**, *44*, 225−229.

https://dx.doi.org/10.1021/acs.jpcc.0c06541